Int J Adv Manuf Technol (2018) 95:973–982
https://doi.org/10.1007/s00170-017-1285-y

ORIGINAL ARTICLE

An approach to predict derivative-chip formation in derivative cutting of micro-textured tools

Ran Duan[1] · **Jianxin Deng**[1] · **Dongliang Ge**[1] · **Xing Ai**[1] · **Yayun Liu**[1] · **Rong Meng**[1] · **Jintao Niu**[1] · **Guijie Wang**[1]

Received: 1 August 2017 / Accepted: 26 October 2017 / Published online: 7 November 2017
© Springer-Verlag London Ltd. 2017

Abstract Derivative cutting of micro-textured tool refers to the additional cutting to the bottom side of the chip with the micro-surface textures on the tool surface. In our previous research, it has been proved that piling up of chip in the microgroove of textures is caused by derivative cutting, resulting in structural function failure of the textured tool face. Hence, derivative-cutting behavior needs to be understood and implemented in models. In this study, an analytical approach for the orthogonal cutting process is developed to determinate derivative-chip formation by predictions of the uncut derivative-chip thickness (UDCT) and minimum uncut derivative-chip thickness (MUDCT) values according to cutting parameters, tool geometry, workpiece material properties, and positional and geometrical parameters of textures. The analytical approach is experimentally validated using a 1045 steel workpiece with the textures of different distances to the main cutting edge on the tool rake face. Subsequently, the responses of the UDCT and MUDCT to cutting speed and texture parameters including its geometry and position are quantified on the basis of the proposed approach. Results show that reasonable enlarging of texture-edge radius and proper increasing of cutting speed both are feasible ways to prevent derivative-cutting from derivative-chip formation.

Keywords Derivative cutting · Derivative-chip formation · Uncut derivative-chip thickness · Minimum uncut derivative-chip thickness

✉ Jianxin Deng
jxdeng@sdu.edu.cn

[1] Department of Mechanical Engineering, Shandong University, Jinan 250061, People's Republic of China

1 Introduction

In recent years, considerable efforts have been made to investigate surface texturing in application of cutting tools; the purpose is to improve tools' cutting performance, such as lowing tool-chip interfacial friction coefficient [1–3], keeping lubricants [4–7], controlling chip flowing [8–11], and reducing wear [12, 13]. Deng et al. [14] developed various types of micro-textures which were filled with MoS_2 solid lubricant on the tool rake face. It was found that the surface texturing can significantly improve the cutting performance, wherein elliptical grooves were more effective compared with parallel or perpendicular grooves. Xing et al. [15] investigated the effects of three types of textures on the cutting performance by orthogonal dry cutting tests on 6061 aluminum alloy tubes, which showed that textured tools can improve the cutting performance, and the rectangular textures was the most effective. Sugihara and Enomoto [16] used femtosecond laser technology to create textured surfaces on cutting tools. As a result, it was revealed that the surface significantly improves the anti-adhesive properties both in wet and dry cutting. Obikawa and Kani [17] found that microgrooves at the tool rake face could change the chip flow direction, resulting in the reduction of cutting forces. Zhang et al. [18] investigated the influence of different lubrication conditions on the cutting performance of textured coated tools. It was found that full lubrication condition can significantly bright advantages of micro-textures on the rake face. Xie et al. [19] investigated the influence of microgrooved tools on cutting temperature and cutting forces in dry turning of titanium alloys. The results showed that the microgrooves on tools could contribute to the decreasing of contact friction on the rake face and reducing of cutting heat. However, the problem associated with the textures plugged by chip material in dry cutting still remains. It results in high affinity between the

slipping chip and chip material in textures and increase in the tool-chip contact area.

To solve the problem described above, different parameters of micro-textured tools such as multiscaled surface textures and hard and/or lubricant coatings have been discussed. For example, Xing et al. [20] demonstrated that the micro-nanoscale textures coated by solid lubricants on the rake face could effectively improve the cutting performance of a conventional Al_2O_3/TiC ceramic tool. They also demonstrated that areal nanotextures combined with soft-coatings were more effective than linear grooves in dry cutting of AISI 1045 steel [21]. Sugihara and Enomoto [22–24] developed a DLC-coated tool with textured surface to determine the role of the textured tool rake face in retaining cutting fluid and decreasing the contact area at the tool-chip interface. The results shown that the nano/micro-textured surface significantly promoted anti-adhesiveness at the tool-chip interface in wet cutting. Zhang et al. [25–27] investigated the effect of surface texturing and burnished solid lubricant on cutting performance of tools with PVD TiAlN films. The wet cutting experiments on AISI 316 austenitic stainless steel showed the fabricating textures on tool surfaces significantly improved the anti-adhesive wear properties of TiAlN-coated tools [26]. Moreover, it was revealed that MoS_2 addition as a solid lubricant could be applied in reduced friction at the tool-chip interface, and microscale textures could prolong the effective life of the initial MoS_2 layer [27]. However, these studies merely alleviated filling of chip in textures when hard and/or lubricant films were coated on the textured surface and in wet cutting. The mechanism for filling of chip in textures was only briefly discussed in only a few studies.

In our previous research [28], microscale textures with a single linear groove parallel to the cutting edge were fabricated on the rake face of the WC/Co cemented carbide tools, and then dry cutting testing on medium carbon steels with the textured tools were conducted. It has been demonstrated that derivative-cutting, additional cutting to the bottom side of the chip with the micro-surface textures on the tool surface, is responsible for the microgroove blocked. The texture-edge with a finite radius acts as a cutting tool to be engaged in the derivative cutting. Owning to limitation of the dimension of the textures, the uncut derivative chip thickness (UDCT) and the texture edge radius are in the same order of magnitude of microscale. It indicates that the removal behavior of derivative cutting is similar to that of micro-cutting. The minimum uncut derivative chip thickness (MUDCT) refers to the minimum bottom side of the chip that can be removed from a chip under ideal performance of the texture edge. In derivative-cutting, a derivative-chip will be generated if the UDCT is larger than a critical value, viz., the MUDCT.

The objective of this paper is to develop an efficient and convenient approach to predict derivative-chip formation in derivative cutting of micro-textured tool by modeling of the UDCT and MUDCT. The modified Oxley's model is utilized to estimate the normal stress distribution and average friction coefficient at the tool-chip interface from given cutting parameters, tool geometry, and material properties. The theory of elasticity has been used as the basic theoretical framework for the prediction of the UDCT values. As integral parts of the model, the positional and geometric parameters of textures, and the normal stress distribution at the tool-chip interface have been taken into accounts. Meanwhile, the MUDCT is found to be functions of the texture edge radius and the friction coefficient based on the micro-cutting theory.

The paper evolves as follows. First, the model development is presented. An iterative method is then proposed to compute the UDCT and MUDCT. The developed model is verified experimentally. Finally, the model is applied to investigate the effect of cutting velocity and the positional and geometric parameters on the UDCT and MUDCT.

2 Model development

In this work, the theory of elasticity will be adopted for prediction for the UDCT. Then, based on the well-established theoretical criterion for transition from plowing to chip formation in micro-cutting, the model for the MUDCT will be established. Finally, an interactive solution method to obtain the UDCT and MUDCT values is based on the modified Oxley's theory.

2.1 Model for uncut derivative chip thickness

The UDCT is determined by analyzing the unique characteristics of the surface height change of the bottom side of the chip. Figure 1 illustrates how a surface height change is generated due to the textures effect. The chip bottom side accesses the point P (see Fig. 1) and begins to be free surface, leading to recovering to the position PTS from the original positon PQR. Then, during the derivative cutting process, the BE edge (see Fig. 6) with finite radius engages the chip material of the shaded area PQRST. As a result, the UDCT refers to the surface height change h at RS. In the considered case of the UDCT, it is not simple to determine exact contours of the surface BCE, and the boundary conditions that make the exact solution of the stated deformation problem is rather difficult. Therefore, simplifications have to be introduced to develop a suitable model. Based on the discussion, modeling of the UDCT can be seen as the solution of a typical nonlinear mechanical problem, deformation of the body (the chip) normally compressed.

All real contact deformations, like all real engineering components, are three-dimensional, and therefore theoretically demand a solution in three-dimensional theory of elasticity or elastoplasticity [29]. But few solutions exist and therefore it is

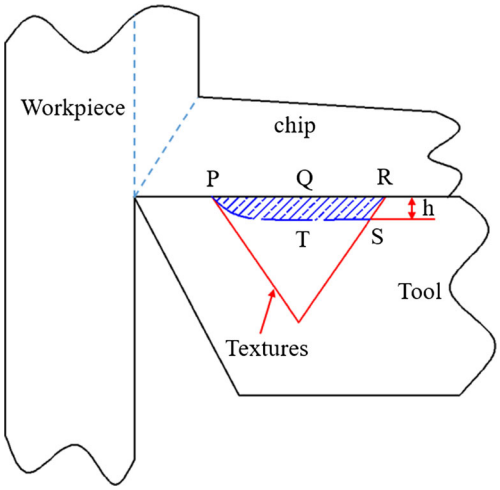

Fig. 1 Schematic diagram of the uncut derivative-chip thickness (UDCT)

feasible to the contact deformation in two dimensions. As known, orthogonal cutting is always considered as a two-dimensional problem [30]. Thus, the investigation of the UDCT is presented in which a three-dimensional problem is reduced to a two-dimension one and thus the calculation is much simplified. Owing to the surface height change accounting for a very small proportion of the chip, the section profiles of the chip can be assumed to be the half-plane, i.e., a semi-infinite body with remote boundary, the normal stress distribution at tool-chip interface is considered as force boundary conditions.

Moving from Boussinesq's problem for the half-plane, the action of a concentrated force p normal to the border $y = 0$ of the elastic half-plane $y > 0$ is considered as shown in Fig. 2. For the plane stress, the y direction displacement vector of U is obtained as follows:

$$v = -\frac{2p}{\pi E}\ln\frac{r_0}{d} - \frac{1+\nu}{\pi E}p \tag{1}$$

where r_0 is the distance from the origin O in the x-direction, E is Young's modulus of elasticity, ν is Poisson's ratio, and d is defined that the y direction displacement vector of symmetry

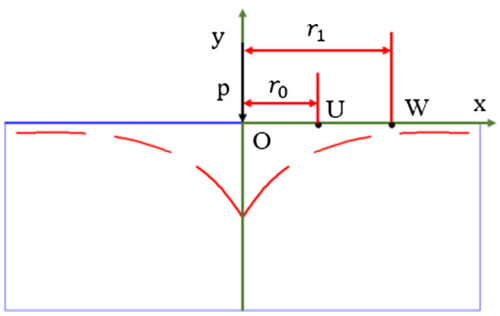

Fig. 2 Schematic diagram of a concentrated force p normal to the border of half-plane

axis Ox tends to zero as $x = d$. Let the other point W (r_1, the distance from the origin O in the x-direction) on the border of the elastic half-plane. The displacement of U relative to point W is as follows:

$$\eta = \left(-\frac{2p}{\pi E}\ln\frac{r_0}{d} - \frac{1+\nu}{\pi E}p\right) - \left(-\frac{2p}{\pi E}\ln\frac{r_1}{d} - \frac{1+\nu}{\pi E}p\right) = \frac{2p}{\pi E}\ln\frac{r_1}{r_0} \tag{2}$$

The next step is to start to build a model that is closer to the real conditions of the surface height change of the bottom side of chip in the textures.

Obviously, plastic flow occurs in a zone adjacent to the tool-chip interface near the cutting edge. Stevenson and Oxley [31] used printed grids (together with an explosive quick-stop device to freeze the chip sections) to measure the plastic flow region in chip formation. The results showed that the thickness of shear zone accounts for a very small proportion of the chip. In addition, plastic deformation is a means of stress relaxation. Based on the above discussion, it indicates that the displacement solution for an elastic half-plane acted by normal pressure should be considered in the analysis of the UDCT. As the previously discussed model provides some insight on the modeling of the displacement solution, the UDCT can be modeled as follows.

The development of the elastic half-plane model is shown in Fig. 3 where the concentrated force is shifted to the normal loading determined by the functions of stress distribution $\sigma_N(x)$. As seen, l_2 is the distance between point W and point U that represents the width of the microgroove of the textures. In addition, ξ is the distance from point U and l_1 is the distance from point U to the cutting edge. As such, the state of relative displacement determined by the infinitesimal force $\sigma_N(l_1 - \xi)d\xi$ is obtained from Eq. 3:

$$dh = \frac{2}{\pi E}\sigma_N(l_1 - \xi)d\xi\ln\frac{\xi + l_2}{\xi} \tag{3}$$

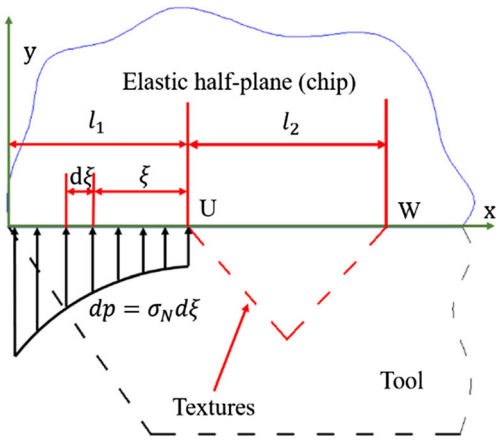

Fig. 3 The mechanics modeling of the UDCT

According to Eq. 3, summing the actions of the infinitesimal force over the $[0, l_1]$ of the boundary, the following expression for the relative displacement function is shown:

$$h = \int_0^{l_1} \frac{2}{\pi E} \sigma_N (l_1 - \xi) d\xi \ln \frac{\xi + l_2}{\xi} d\xi \tag{4}$$

In order to obtain the relative displacement h to predict the UDCT value, the functions of normal stress distribution σ_N at the tool-chip interface is required.

2.2 Model for minimum uncut derivative thickness

According to our previous work [28], it has been found that the uncut derivative chip thickness (UDCT) in the micron level is comparable in size to the radius of the texture edge. Based on the micro-cutting theory [32, 33], introduction of the minimum uncut derivative chip thickness (MUDCT) is used for determination of derivative chip formation, under which the chip bottom side material is not removed but plowed. The stagnation or neutral angle for the corresponding minimum uncut chip thickness, which is defined by some researcher [34–36], contributes to modeling of the MUDCT. A schematic of material flow around a texture edge with a finite radius is shown in Fig. 4. A stagnant point S is supposed on the rounded texture-edge, below which the material flows downward without any derivative-chip formation. This phenomenon is called plowing, which is elastic-plastic deformation without material removal. Above this stagnation point, the material flows up and forms as derivative-chip. According to the geometric relationship between stagnant angle θ_s and effective negative rake angle $\alpha_s = \pi/2 - \theta_s$, the value of the minimum uncut chip thickness can be determined, namely:

$$h_{\mathrm{m}} = r_{\mathrm{e}}(1 - \cos\theta_{\mathrm{s}}) \tag{5}$$

where r_{e} is the edge radius. A micro-cutting model proposed by Son et al. [35] was that the tool edge radius and the friction coefficient at the tool-chip interface governed the minimum cutting thickness, wherein the stagnant angle can be determined based on the friction angle, namely:

$$\theta_{\mathrm{s}} = \frac{\pi}{4} - \frac{\beta_{\mathrm{s}}}{2} \tag{6}$$

where β_{s} is the friction angle. In this paper, the minimum uncut chip thickness model can be used for the estimation of the MUDCT values. Meanwhile, derivative cutting occurs at the tool-chip interface. The friction angle β_{s} can be approximately equal to that at the tool-chip interface. Thus, in order to obtain β_{s}, the average friction coefficient at the tool-chip interface is required.

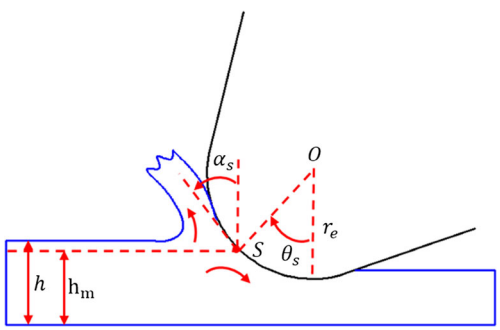

Fig. 4 Machining using an edge radius tool

2.3 Solution for the UDCT and MUDCT values

To determine the UDCT and MUDCT, the distributions of normal stress and average friction coefficient at the tool-chip interface should be acquired. With the increasing insight into the mechanism of macro-cutting, this goal can be achieved. For macro-cutting, two fundamental approaches have been extensively researched [37]: (1) the minimum energy principle and (2) the slip line field theory. Oxley and co-workers [31] made the most significant contribution to the field by introduction of the parallel-sided zone theory, flow stress, and thermal properties of workpiece material, tool geometry, and cutting conditions were taken into account to predict forces, temperatures, and stresses in the deformation zones [38, 39]. The Oxley's model can be used in combination with various material constitutive laws, and hence the Johnson-Cook (JC) constitutive model [40] is chosen to determine shear flow stress. This enables us to predict distribution of normal stress and frictional coefficient along the tool-chip interface directly from material properties, tool geometry, and cutting conditions.

For representation of workpiece material behavior under high-speed cutting conditions, Johnson and Cook proposed the constitutive model to introduce a semi-empirical function of temperature, strain and strain rate to describe the flow stress of material as given in Eq. (7).

$$\overline{\sigma} = \left[A + B\left(\overline{\varepsilon}\right)^n\right]\left[1 + C\ln\frac{\dot{\overline{\varepsilon}}}{\dot{\overline{\varepsilon}}_0}\right]\left[1 - \left(\frac{T - T_0}{T_m - T_0}\right)^m\right] \tag{7}$$

The constants A, B, C, n, and m of the model are obtained by Split Hopkinson Pressure Bar (SHPB) tests conducted at strain ranges of 0.05 to 0.2, strain-rate of 7500 1/s, and temperature ranges of 35 to 625 °C by Jaspers and Dautzenberg [41] for AISI 1045 steel as given in Table 1.

The next step is to reveal a predicted approach based on Oxley's model and the Johnson-Cook model to acquire normal stress distributions and average of the friction coefficient at the tool-chip interface directly from the workpiece material

Table 1 Johnson-Cook material constants obtained from SHPB tests

Material	T_m (°C)	A (MPa)	B (MPa)	C	n	m
AISI 1045	1460	553.1	600.8	0.0134	0.234	1

properties, tool geometry, and cutting conditions. For the orthogonal cutting model, the shear angle ϕ, strain rate constant C_0, and the ratio δ of thickness of the tool-chip interface plastic zone to chip thickness are essential parameters that can be used for predicting other output values, such as tool-chip contact length, cutting force, and distribution of stress and temperature in deformation zones. The shear angle ϕ is determined according to the fact that the tool-chip interface shear stress (Eq. 8) caused by the resultant cutting force for a given set of cutting conditions should be equal to the chip material flow stress k_{chip} (Eq. 9) at the sticking region, which is obtained from the J-C constitutive model. Equations 8 and 9 are shown as follows:

$$\tau_{\text{int}} = \frac{F}{\chi l_c w} \tag{8}$$

where F is the frictional force between the chip and the tool, χ represents the ratio of the distance from the cutting edge to the point where the resultant force R intersects the tool rake face, l_c is the contact length along the tool-chip interface, and w is the cutting width. The flow stress at the tool-chip interface K_{int} can be found by utilizing Eq. 7:

$$K_{\text{int}} = \frac{1}{\sqrt{3}}\left[A + B\left(\bar{\varepsilon}_{\text{int}}\right)^n\right]\left[1 + C\ln\frac{\dot{\bar{\varepsilon}}_{\text{int}}}{\dot{\bar{\varepsilon}}_0}\right]\left[1-\left(\frac{T_{\text{int}}-T_0}{T_m-T_0}\right)^m\right] \tag{9}$$

where $\bar{\varepsilon}_{\text{int}}$, $\dot{\bar{\varepsilon}}_{\text{int}}$, and T_{int} are the plastic equivalent strain, the equivalent plastic strain rate, and the temperature at the second zone, respectively. C_0 is a constant representing the ratio of the thickness of the primary zone to the length of plane, which can be found by satisfying the condition that the average value of normal stress at the tool-chip interface is equal to the normal stress at the point B of the cutting edge. The average value of normal stress at the tool-chip interface is given as:

$$\sigma_N = \frac{N}{w l_c} \tag{10}$$

where N is the normal component of the resultant cutting force. Meanwhile, the normal stress at the point B of cutting edge can be obtained as:

$$\sigma_N{}' = K_{AB}\left(1 + \frac{\pi}{2} - 2\alpha - 2C_O n\frac{B\varepsilon_{AB}^n}{A + B\varepsilon_{AB}^n}\right) \tag{11}$$

where k_{AB} is the flow stress along the plane AB calculated by using Eq. 10 and Eq. 11, ε_{AB} is the equivalent plastic strain on the plane AB. The ratio δ of thickness of the tool-chip interface plastic zone to chip thickness is selected based on the minimum force principle.

According to Zorev [42], normal stress is greatest at the tool tip and gradually decreases to zero at the point where the chip separates from the rake face. Normal stress distribution on the tool rake face is modeled as a power-law relationship. The normal stress distribution on the bottom side of the chip can be described by Eq. 12:

$$\sigma_N(x) = \sigma_{N_{\max}}\left[1-\left(\frac{x}{l_c}\right)^a\right] \tag{12}$$

In Eq. 12, x is the distance from main cutting edge, and a is the power exponent. The component values of Eq. 12 and the average friction coefficient μ at the tool-chip interface can be determined from the following equations:

$$\sigma_{N_{\max}} = K_{AB}\left(1 + \frac{\pi}{2} - 2\alpha - 2C_O n\frac{B\varepsilon_{AB}^n}{A + B\varepsilon_{AB}^n}\right) \tag{13}$$

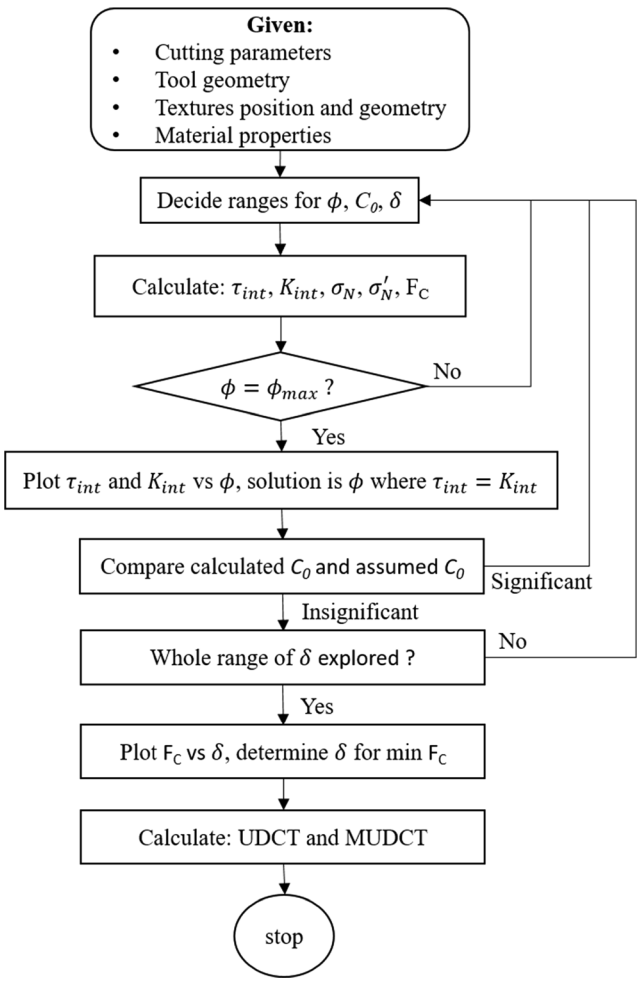

Fig. 5 Simplified flow chart of the iterative solution method

Table 2 Experimental parameters of the Nd/YAG laser used during irradiation of WC/Co cemented carbide tool

Pump current (A)	8.6
Frequency (KHz)	20
Scanning speed (mm/s)	60
Number of overscan	1

$$a = \frac{F_N}{wl_c\left(1+\frac{\pi}{2}-2\alpha-2\frac{BnC_O}{A+B\varepsilon_{AB}^n}\right)-F_N} \tag{14}$$

$$l_c = \frac{t_u \sin\theta}{\cos\lambda\sin\phi}\left(1+\frac{C_O n}{3\left[1+2\left(\frac{\pi}{4}-\phi\right)-C_O n\right]}\right) \tag{15}$$

$$\mu = \tan\lambda \tag{16}$$

where the angle λ and θ are given with Eq. 17 and Eq. 18.

$$\tan\theta = 1+2\left(\frac{\pi}{4}-\phi\right)-C_O n \tag{17}$$

$$\lambda = \theta-\phi+\alpha \tag{18}$$

Figure 5 shows the simplified flow chart of the iterative solution method to obtain the UDCT and MUDCT values by considering the workpiece material properties, tool geometry, cutting parameters, and positional and geometrical parameters of textures. It indicates that the UDCT and MUDCT are coupled with strain, strain rate, and temperature in a complicated manner.

3 Experimental setup

In order to investigate the proposed models, several experimental cutting tests are performed. The dry cutting tests are carried out on a lathe equipped with a Kennametal 2525M3 tool holder, with a rake angle 0°, clearance angle 7°, and inclination angle 0°. An Nd/YAG laser (DP-H50, Jinan Xinchu Co., China) with a wavelength of 1064 nm and pulse duration of 10 ns is used for texturing of the rake face of inserts (Type: NG3189 K420, Kennametal Inc., USA). The processing parameters of the Nd/YAG laser are given in Table 2. Figure 6 shows a schematic diagram of microscale textures of the textured tool. The type of textures is designed as a single line with the direction of textures parallel to the cutting edge. As shown in this figure, the width of the microscale groove is about 50 μm, the depth of textures is about 35 μm, and the distance L to the main cutting edge respectively are 150, 200, 250, 300, and 350 μm. To simplify the nomenclature, the tools with textures of the distance to the main cutting edge 150, 200, 250, 300, and 350 μm are named TT-150, TT-200, TT-250, TT-300, and TT-350, respectively. Figure 7 shows an example of the three-dimensional image of the textures examined by an optical microscope (KEYENCE, Japan). The BE edge radius r_e of the textures is examined five times as shown in Fig. 7b and the average value is approximately 5 μm.

The experimental setup is shown in Fig. 8. Orthogonal cutting tests are conducted on a CA6140 lathe equipped with the textured tools. The workpiece material was AISI 1045 steel with a hardness of HRC 19–31 in the form of pre-cut disk with an external diameter of 100 mm. All tests are carried out with the following parameters: cutting speed v = 90 m/min, feed rate f = 0.1 mm/rev, and width of cut a_w = 2 mm. This provided a plane strain condition for cutting; therefore, the results are assumed independent to the width of cutting.

As the textures is located at the tool-chip interface, it is difficult to directly observe the unique characteristics of derivative-chip formation in the cutting process. However, due to the derivative cutting as a type of micro-cutting, the derivative chip can flow from the BE edge into the microgroove, leading to blocking of the textures with chip material. Therefore, the morphology of the derivative chip in textures and the bottom side of the chip can be detected by a scanning electron microscope (SEM, QUANTA FEG 250, FEI Inc., USA).

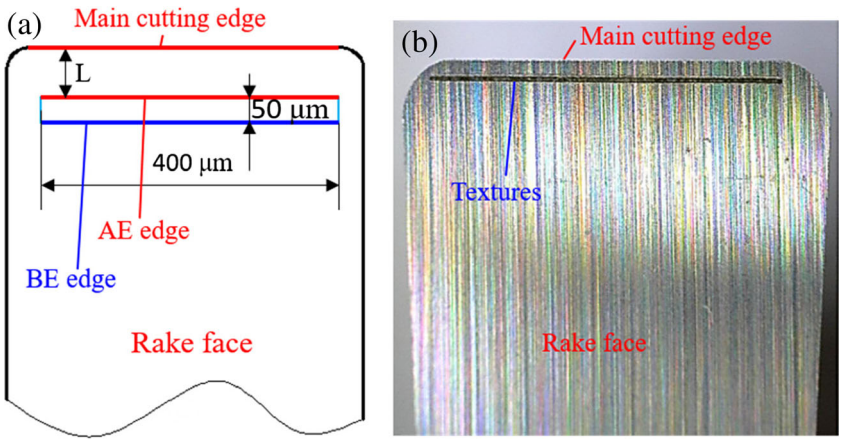

Fig. 6 A developed cutting tool with microscale textures. **a** Schematic diagram of the microscale textures with geometrical and positional characteristics on the rake face of cutting tools. **b** Optical image of the rake face

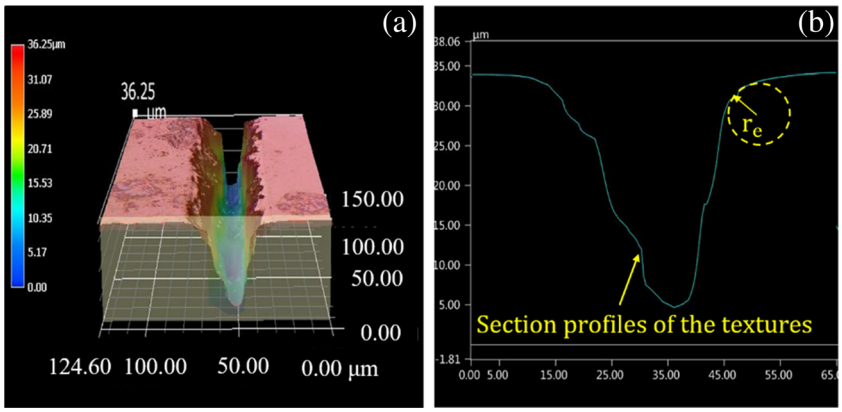

Fig. 7 **a** Three-dimensional optical image of the microscale textures. **b** The corresponding sectional profiles of the textures

4 Results and discussions

4.1 Model validation

Figure 9 shows the simulated UDCT and MUDCT for machining 1045 steel with the textures of different distance L to the main cutting edge. From Fig. 9, the model predicts that the UDCT decreases as the distance L increases. Within the range of 150–250 μm, the value of UDCT exceeds the MUDCT, which illustrates that not only plowing occurs but also continuous derivative chips are generated. When the distance L changes from 300 to 350 μm, the UDCT begins to be near even slightly below MUDT. Under this state, the derivative-cutting process is dominated by plowing, which is a type of plastic deformation of the chip material without continuous derivative-chip formation.

Figure 10 shows the variations in the amount of derivative chip adhering in the textures for the TT-150, TT-200, TT-250, TT-300, and TT-350 tools. It is observed that, for the TT-150, TT-200, and TT-250 tools, derivative chip fully piles up in the textures, as can be seen from Fig. 10a–c. For the TT-300 and TT-350 tools, the amount of derivative-chip in the textures is obviously less as shown in Fig. 10d–e, especially for the TT-350 tool, a part of the surface of textures remains visible. It can be explained that, once the plowing process tends to be significant, the phenomenon of derivative-chip formation is alleviated. In addition, at the critical state to the plowing process of derivative cutting, the chip material piles up in front of the BE edge; and, when the thickness of the piled-up material reaches a critical value (MUDCT), discontinuous chip is generated. Therefore, a small amount of derivative chip can be adhered to the surface of the texture as shown in Fig. 10e. Meanwhile, this behavior is a strong indication for the formation of built-up edges. Built-up edges can exist on the surface of the workpiece (the bottom side of the chip in this study) confirmed by Autenrieth [43], leading to higher surface roughness. Thus, comparing the surface morphology of the bottom side of the chip obtained with the five types of tools is shown in Fig. 11. It appears that built-up edges remain visible on the bottom sides of the chips for TT-300 and TT-350 tools, and the size of the built-up edges for TT-350 is larger than that for TT-300, which validates the above discussion about formation of a built-up edge owing to plowing phenomena involving strong plastic deformation of the chip material. Based on the experimental results, the distance L around between 300 and 350 μm characterizes the transition from derivative-chip formation to plowing with discontinuous chip formation. Therefore, the proposed models for the UDCT

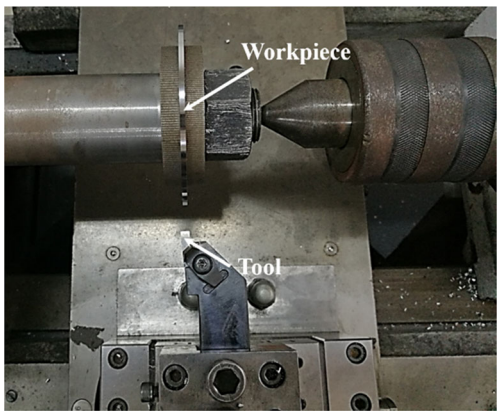

Fig. 8 Experimental setup of orthogonal cutting with the micro-textured tools

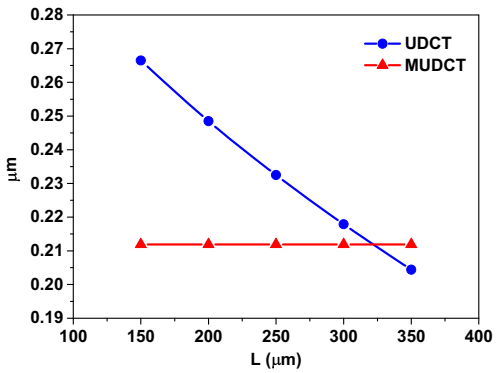

Fig. 9 Predicted UDCT and MUDCT in different distance L of the textures to the main cutting edge

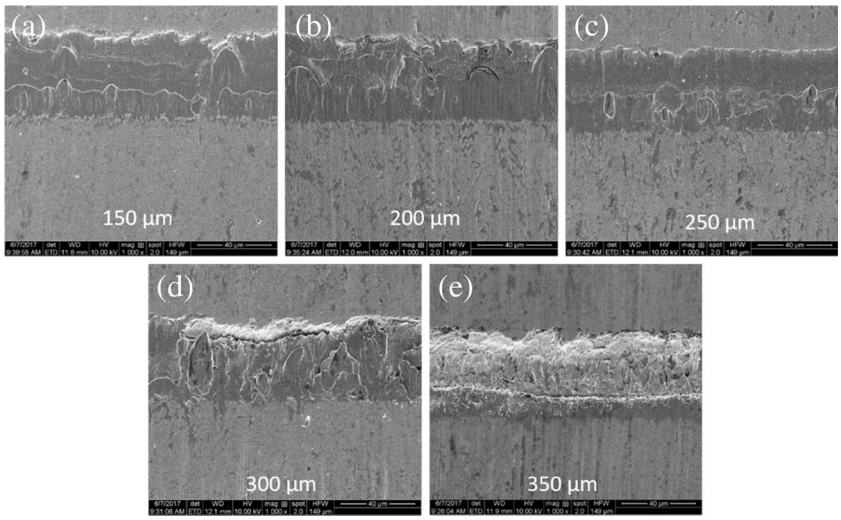

Fig. 10 Wear track of textures with different distances to the main cutting edge (150 μm 200 μm, 250 μm, 300 μm, 350 μm)

and MUDCT show the similar trends as the experimental tests with cutting tools with the textures of different distances to the main cutting edge.

4.2 Effect of cutting speed

According to Figs. 12 and 13, the simulated UDCT and MUDCT are both increased with the increase of cutting speed. Determination of the MUDCT and UDCT depends on the modified Oxley theory, and so the MUDCT and UDCT are influenced by the temperature, strain, and strain rate at the tool-chip interface. Meanwhile, the increased cutting speed influences the chip material behavior in two ways [44]. First one, the increase of cutting speed leads to the thermal softening effecting increasing, resulting in the ductility of the bottom side of the chip increasing. This would cause the MUDCT and UDCT increasing. The other one, the effective strain and strain rate of the chip are also increased with increase of cutting velocity, contributing to enhancement of the strain-harden and reduction of the ductility. This would cause the MUDCT and UDCT to decrease. Based on the above analyses, the thermal softening effect is dominant for the MUDCT and UDCT compared with the strain-harden effect. In addition, with generally increasing of the cutting velocity under BE edge radius above 5 μm, the UDCT values can be significantly less than the MUDCT as shown in Figs. 12 and 13, leading to plowing without any derivative-chip formation in derivative cutting. Therefore, the chip material becomes more ductile and more difficult to form derivative-chips as the cutting speed increases.

It also can be seen from Fig. 13 that for the MUDCT, as the cutting speed increases to around 210 m/min, the decrease in the MUDCT is much in evidence, but as the temperature increases to a certain range, the flow stress increases with the increased temperature. This effect is well known to be caused by dynamic strain aging and is termed “blue brittleness” [31]. As is shown in the simulation study, blue brittleness affects the relationship between the MUDCT and the cutting velocity.

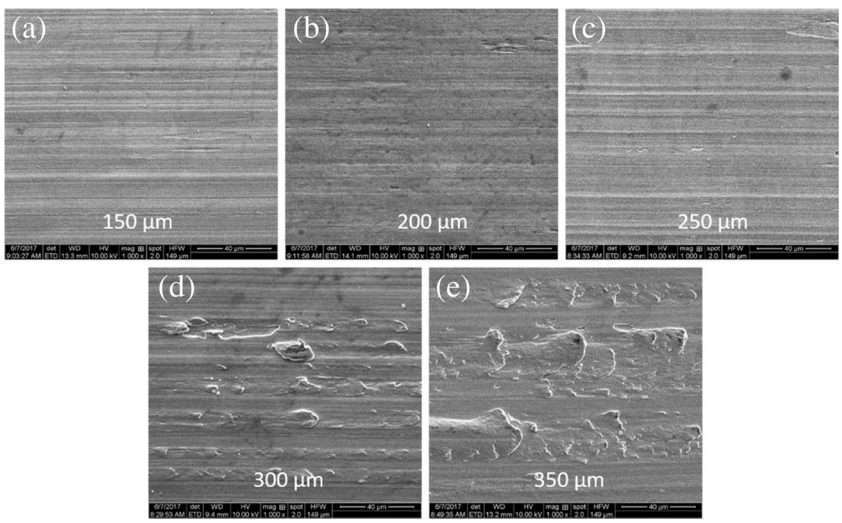

Fig. 11 Surface morphology of the bottom side of the chip for the textures with different distances to the main cutting edge (150 μm, 200 μm, 250 μm, 300 μm, 350 μm)

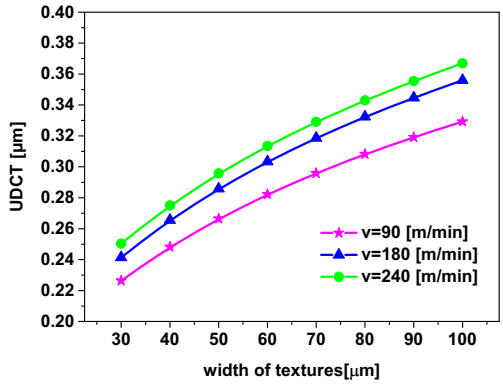

Fig. 12 Effects of the cutting velocity and width of textures on the UDCT under condition of the distance L of 150 μm

4.3 Effect of positional and geometrical parameters of textures

Figures 9, 12, and 13 show that the positional and geometrical parameters of textures also have a profound effect on the MUDCT and UDCT based on simulated results. Normal stress distribution on the tool rake face is modeled as a power-law relationship, wherein normal stress is greatest at the tool tip and gradually decreases to zero at the point where the chip separates from the rake face. Therefore, according to Eq. (4), the increased distance of the textures to the main cutting edge contributes to the decrease of the normal stress, resulting in the UDCT decreasing as shown in Fig. 9. In addition, the increased width of textures leads to relative displacement between the points E and F (see Fig. 3) increasing, causing the UDCT increasing as shown in Fig. 12. In addition, as the BE edge radius increases, the MUDCT increases as shown in Fig. 13. Due to the increasing of the BE edge radius, plowing in the cutting process is more dominant. This brings out higher energy dissipation and cutting temperatures [45], making the material more ductile. Therefore, the MUDCT tends to be higher.

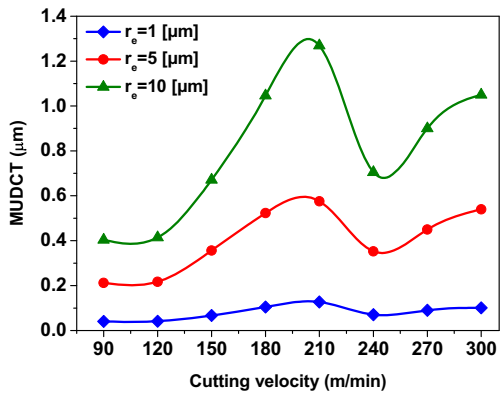

Fig. 13 Effects of the cutting velocity and the BE edge radius on the MUDCT under condition of the texture width of 50 μm and distance L of 150 μm

Obviously, the larger distance of textures to the main cutting edge and smaller width of textures can cause lower UDCT, but these may not effectively bring about the beneficial effects of surface texturing on the cutting performance such as reduction in friction and resistance of tool wear. Therefore, reasonable enlarging of the BE edge radius and proper increasing of the cutting velocity both are feasible ways to prevent derivative cutting from chip formation.

5 Conclusions

Based on our previous work, derivative cutting of micro-textured tools means the additional removal of material from chip the bottom side with tool surface textures, leading to high power consumption in the cutting process. In addition, formation of derivative-chip can cause blocking of the microgroove, resulting in the structural function failure of the textures. Hence, derivative-cutting behavior needs to be understood and implemented in models. The following conclusions can be drawn from this paper:

(1) An analytical approach for the orthogonal cutting process is introduced to conveniently predict whether or not derivative-chip is generated in derivative cutting by determination of the UDCT and MUDCT values according to cutting parameters, tool geometry, workpiece material properties, and positional and geometrical parameters of textures.
(2) The analytical approach is experimentally validated using a 1045 steel workpiece with the textures of different distances to the main cutting edge on the tool rake face.
(3) The approach is applied to investigate the effects of cutting velocity and the positional and geometric parameters on the UDCT and MUDCT. Results show that reasonable enlarging of the texture-edge radius and proper increasing of the cutting velocity both are feasible ways to prevent derivative-cutting from derivative-chip formation.

Acknowledgements This work is supported by the National Natural Science Foundation of China (51675311) and Development Plan of Science and Technology of Shandong Province (2017GGX30115).

References

1. Xie J, Luo M, He J, Liu X, Tan T (2012) Micro-grinding of micro-groove array on tool rake surface for dry cutting of titanium alloy. Int J Precis Eng Manuf 13:1845–1852
2. Ma J, Duong H, Lian Y, Lei S (2015) Assessment of microgrooved cutting tool in dry machining of AISI 1045 steel. J Manuf Sci Eng 137:031001

3. Deng J, Lian Y, Wu Z, Xing Y (2013) Performance of femtosecond laser-textured cutting tools deposited with WS_2, solid lubricant coatings. Surf Coat Technol 222:135–143
4. Ling T, Liu P, Xiong S, Grzina D, Cao J, Wang J, Xia C, Talwar R (2013) Surface texturing of drill bits for adhesion reduction and tool life enhancement. Tribol Lett 52:113–122
5. Li Y, Deng J, Chai Y, Fan W (2016) Surface textures on cemented carbide cutting tools by micro EDM assisted with high-frequency vibration. Int J Adv Manuf Technol 82:2157–2165
6. Enomoto T, Sugihara T (2011) Improvement of anti-adhesive properties of cutting tool by nano/micro textures and its mechanism. Procedia Eng 19:100–105
7. Jahan M, Rahman M, Wong Y (2011) A review on the conventional and micro-electrodischarge machining of tungsten carbide. Int J Mach Tools Manuf 51:837–858
8. Xie J, Li Y, Yang L (2015) Study on 5-axial milling on microstructured freeform surface using the macro-ball cutter patterned with micro-cutting-edge array. CIRP Ann Manuf Technol 64:101–104
9. Kumar Pal V, Choudhury SK (2014) Fabrication and analysis of micro-pillars by abrasive water jet machining. Procedia Mater Sci 6:61–71
10. Chang W, Sun J, Luo X (2011) Investigation of microstructured milling tool for deferring tool wear. Wear 271:2433–2437
11. Lei S, Devarajan S, Chang Z (2009) A study of micropool lubricated cutting tool in machining of mild steel. J Mater Process Technol 209:1612–1620
12. Lei S, Devarajan S, Chang Z (2009) A comparative study on the machining performance of textured cutting tools with lubrication. J Mater Process Technol 2:401–413
13. Fatima A, Mativenga P (2015) A comparative study on cutting performance of rake-flank face structured cutting tool in orthogonal cutting of AISI/SAE 4140. Int J Adv Manuf Technol 78:2097–2106
14. Deng J, Wu Z, Lian Y, Qi T, Cheng J (2012) Performance of carbide tools with textured rake-face filled with solid lubricants in dry cutting processes. Int J Refract Met Hard Mater 30:164–172
15. Xing Y, Deng J, Wang X, Ehmann K, Cao J (2016) Experimental assessment of laser textured cutting tools in dry cutting of aluminum alloys. J Manuf Sci Eng 138:071006
16. Sugihara T, Enomoto T (2012) Improving anti-adhesion in aluminum alloy cutting by micro stripe texture. Precis Eng 36:229–237
17. Obikawa T, Kani B (2012) Micro ball end milling of titanium alloy using a tool with a microstructured rake face. JAMDSM 6:1121–1131
18. Zhang K, Deng J, Xing Y, Li S, Gao H (2015) Effect of microscale texture on cutting performance of WC/Co-based TiAlN coated tools under different lubrication conditions[J]. Appl Surf Sci 326:107–118
19. Xie J, Luo M, Wu K, Yang L, Li D (2015) Experimental study on cutting temperature and cutting force in dry turning of titanium alloy using a non-coated micro-grooved tool. Int J Mach Tools Manuf 73:25–36
20. Xing Y, Deng J, Zhao J, Zhang G, Zhang K (2014) Cutting performance and wear mechanism of nanoscale and microscale textured Al_2O_3/TiC ceramic tools in dry cutting of hardened steel. Int J Refract Met Hard Mater 43:46–58
21. Xing Y, Deng J, Li S, Yue H, Meng R, Gao P (2014) Cutting performance and wear characteristics of Al_2O_3 /TiC ceramic cutting tools with WS_2/Zr soft-coatings and nano-textures in dry cutting. Wear 318(1–2):12–26
22. Enomoto T, Watanabe T, Aoki Y, Ohtake N (2007) Development of a cutting tool with micro structured surface. Nippon Kikai Gakkai Ronbunshu C Hen/Trans Jpn Soc Mech Eng C 73:1560–1565
23. Enomoto T, Sugihara T (2010) Improving anti-adhesive properties of cutting tool surfaces by nano−/micro-textures. CIRP Ann Manuf Technol 59:597–600
24. Sugihara T, Enomoto T (2009) Development of a cutting tool with a nano/micro-textured surface-improvement of anti-adhesive effect by considering the texture patterns. Precis Eng 33:425–429
25. Zhang K, Deng J, Meng R, Gao P, Yue H (2015) Effect of nano-scale textures on cutting performance of WC/Co-based $Ti_{55}Al_{45}N$ coated tools in dry cutting. Int J Refract Met Hard Mater 51:35–49
26. Zhang K, Deng J, Sun J, Jiang C, Liu Y (2015) Effect of micro/nano-scale textures on anti-adhesive wear properties of WC/Co-based TiAlN coated tools in AISI 316 austenitic stainless steel cutting. Appl Surf Sci 355:602–614
27. Zhang K, Deng J, Lei S, Yu X (2016) Effect of micro/nano-textures and burnished MoS_2, addition on the tribological properties of PVD TiAlN coatings against AISI 316 stainless steel. Surf Coat Technol 291:382–395
28. Duan R, Deng J, Ai X, Liu Y, Chen H (2017) Experimental assessment of derivative cutting of micro-textured tools in dry cutting of medium carbon steels. Int J Adv Manuf Technol 92:3531–3540
29. Hills D, Nowell D, Sackfield A (1993) Mechanics of elastic contacts. Butterworth Heinemann, London
30. Zorev N (1958) Results of work in the field of the mechanics of the metal cutting process, Proceedings of the IME Conf Tech Eng Manuf, London, 255
31. Oxley P (1989) The mechanics of machining: an analytical approach to assessing machinability. Ellis Horwood, Chichester
32. Kim C, Bono M, Ni J (2002) Experimental analysis of chip formation in micromilling. Trans NAMRI 129:247–254
33. Chae J, Park S, Freiheit T (2006) Investigation of micro-cutting operations. Int J Mach Tools Manuf 46:313–332
34. Malekian M, Mostofa M, Park S, Jun M (2012) Modeling of minimum uncut chip thickness in micro machining of aluminum. J Mater Process Technol 212:553–559
35. Son S, Han S, Ahn J (2005) Effects of the friction coefficient on the minimum cutting thickness in micro cutting. Int J Mach Tools Manuf 45:529–535
36. Yuan Z, Zhou M, Dong S (1996) Effect of diamond tool sharpness on minimum cutting thickness and cutting surface integrity in ultraprecision machining. J Mater Process Technol 62:327–330
37. Karpat Y, Özel T (2006) Predictive analytical and thermal modeling of orthogonal cutting process—part I: predictions of tool forces, stresses, and temperature distributions. J Manuf Sci Eng 128:33–36
38. Childs T (1998) Material property needs in modeling metal machining. Mach Sci Technol 2:303–316
39. Özel T, Altan T (2000) Determination of workpiece flow stress and friction at the chip–tool contact for high-speed cutting. Int J Mach Tools Manuf 40(1):133–152
40. Johnson G, Cook W (1983) A constitutive model and data for metals subjected to large strains, high strain rates and high temperatures. Proceedings of the 7th International Symposium on Ballistics 21: 541–547
41. Jaspers S, Dautzenberg J (2002) Material behaviour in conditions similar to metal cutting: flow stress in the primary shear zone. J Mater Process Technol 122:322–330
42. Zorev N (1963) Inter-relationship between shear processes occurring along tool face and shear plane in metal cutting. Int Res Prod Eng:42–49
43. Autenrieth H (2010) Numerische Analyse der Mikrozerspanung am Beispiel von normalisiertem C45E [M]. Shaker, Aachen
44. DeVor R, Kapoor S (2004) On the modeling and analysis of machining performance in micro-endmilling, part I: surface generation. J Manuf Sci Eng 126:685–694
45. Liu X, DeVor R, Kapoor S (2006) An analytical model for the prediction of minimum chip thickness in micromachining. J Manuf Sci Eng 128:474–481